LA-5038

No. 2443

Nonlinear Radiation Transport Simulation with an Implicit Monte Carlo Method

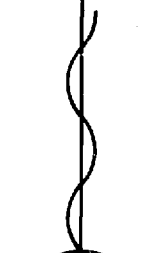

los alamos
scientific laboratory
of the University of California
LOS ALAMOS, NEW MEXICO 87544

MASTER

UNITED STATES
ATOMIC ENERGY COMMISSION
CONTRACT W-7405-ENG. 36

Printed in the United States of America. Available from
National Technical Information Service
U. S. Department of Commerce
5285 Port Royal Road
Springfield, Virginia 22151
Price: Printed Copy $3.00; Microfiche $0.95

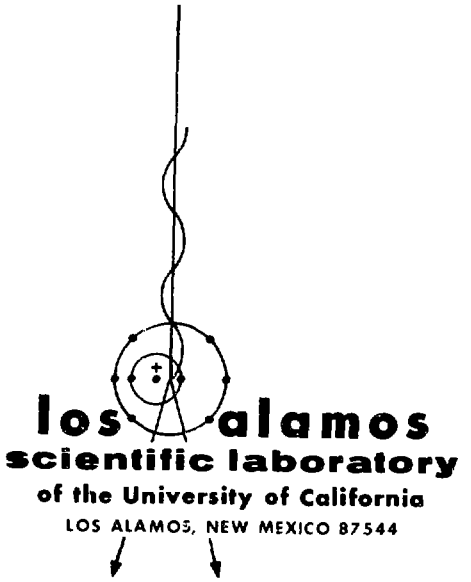

LA-5038
UC-32
ISSUED: January 1973

Nonlinear Radiation Transport Simulation with an Implicit Monte Carlo Method

by

L. L. Carter
C. A. Forest

NONLINEAR RADIATION TRANSPORT SIMULATION WITH AN IMPLICIT MONTE CARLO METHOD

by

L. L. Carter and C. A. Forest

ABSTRACT

A method is developed to solve the radiative transport equation with Monte Carlo. The photon source aT^4 is expressed as the sum of an extraneous source term plus a pseudoscattering term by utilizing the radiative energy balance equation. This resulting photon source is sampled directly in the Monte Carlo calculation with an extrapolation of cross sections and equation-of-state data from the previous time step.

I. INTRODUCTION

An implicit Monte Carlo method has been reported recently by Fleck and Cummings[1] and by Fleck[2] for the simulation of nonlinear radiation transport. They used an effective scattering technique to gain improved accuracy and to incorporate stability in the calculation. The results of preliminary calculations by Fleck and Cummings indicated that their proposed method has better stability characteristics than a previously reported fully explicit calculation.[3] Later calculations indicate improved accuracy provided opacities and equation-of-state data are extrapolated in a proper manner.

The purpose of this report is to propose an implicit Monte Carlo method that appears to have certain advantages over the method of Fleck and Cummings. Specifically, a more exact treatment of the coupling between the material energy density equation and the transport equation is provided, which should enable the use of longer mesh intervals in time, an important statistical consideration. This method also removes the time centering parameter α that was present in Fleck and Cummings' method.

The mathematical formulation of the radiative transport is discussed in Sec. II. An implicit Monte Carlo method for solving the radiative transport problem in the absence of scattering is given in Sec. III. In Sec. IV, some numerical results of applying the implicit method of Sec. III on some example problems are given. The implicit Monte Carlo method is generalized further in Sec. V to include scattering. The treatment of inverse Compton scattering with Monte Carlo is discussed in Sec. VI.

II. MATHEMATICAL DESCRIPTION OF RADIATIVE TRANSPORT

General Discussion

The mathematical description of radiative transport is discussed in considerable detail by Pomraning.[4] The paper by Pomraning provides a good reference for the approximations involved in various mathematical descriptions of radiative transport, therefore we will omit such a discussion here. For our purposes we will utilize the transport equation in the form

$$\frac{1}{c}\frac{\partial I(R)}{\partial t} + \underline{\Omega}\cdot\underline{\nabla} I(R) + \mu_t(\nu)\, I(R) = \mu_a(\nu)\, B(\nu)$$

$$+ \int\int \frac{\nu}{\nu'}\, \mu_s(\nu'\to\nu, \underline{\Omega}\cdot\underline{\Omega}')\, I(\underline{r},\nu',\underline{\Omega}',t)\, d\nu'\, d\underline{\Omega}', \quad (1)$$

where R is a shorthand notation denoting a space position $\underline{r}$, a direction of flight $\underline{\Omega}$, and a frequency ν at time t. I(R) is the specific intensity, and B(ν) is the Planck function,

$$B(\nu) = \frac{2h\nu^3}{c^2} \frac{1}{\left(e^{h\nu/kT} - 1\right)} \quad , \tag{2}$$

where μ_a is the absorption coefficient corrected for induced effects as

$$\mu_a(\nu) = \mu_a'(\nu)/[1 + c^2 B(\nu)/2h\nu^3] \quad , \tag{3}$$

and μ_t is the total attenuation coefficient

$$\mu_t(\nu) = \mu_a(\nu) + \int\int \mu_s(\nu \to \nu', \Omega \cdot \Omega') d\nu' d\underline{\Omega}' \quad . \tag{4}$$

We have assumed local thermodynamic equilibrium to obtain the transport equation in the form of Eq. (1). In addition, induced processes have been neglected in the scattering terms. The variables μ_a, μ_t, μ_s, and B also depend upon spatial position and time, but this has been suppressed in the interest of compacting notation.

The transport equation is coupled through the emission source term to a radiation and material energy balance. The equation to express energy conservation is

$$\frac{\partial u_r(\underline{r},t)}{\partial t} = \beta(\underline{r},t) \left\{ \left[\int\int \mu_t(\nu)\, I(R) d\nu\, d\underline{\Omega} \right] - \left[\int\int\int\int \frac{\nu}{\nu'} \mu_s(\nu' \to \nu, \underline{\Omega} \cdot \underline{\Omega}')\, I(\underline{r}, \nu', \underline{\Omega}', t) d\nu d\underline{\Omega} d\nu' d\underline{\Omega}' \right] - c\, \sigma_p(\underline{r},t)\, u_r(\underline{r},t) + S(\underline{r},t) \right\} \quad , \tag{5}$$

where $u_r(\underline{r},t)$ is the equilibrium radiation energy density* defined in terms of the Planck function as

$$u_r(\underline{r},t) = \frac{4\pi}{c} \int B(\nu) d\nu = aT^4 \tag{6}$$

with

$$a = \frac{32k^4\pi^5}{60c^3h^3} \quad . \tag{7}$$

The emission term in the transport equation will subsequently be expressed in terms of the radiation energy density as

$$\mu_a(\nu)\, B(\nu) = \frac{c}{4\pi} \mu_a(\nu)\, b_\nu\, u_r(\underline{r},t) \quad , \tag{8}$$

where b_ν is the normalized Planck spectrum

$$b_\nu = \frac{15h^4\nu^3}{\pi^4 k^4 T^4} \frac{1}{\left[e^{h\nu/kT} - 1\right]} \quad . \tag{9}$$

This enables us to define the σ_p in Eq. (5) in terms of b_ν as

$$\sigma_p(\underline{r},t) = \int b_\nu\, \mu_a(\nu)\, d\nu \quad . \tag{10}$$

The remaining variables, not yet defined in Eq. (5), are an arbitrary source function S and the variable β that relates the material energy density u_m to the radiation energy density u_r as

$$\frac{\partial u_m(\underline{r},t)}{\partial u_r(\underline{r},t)} = \frac{1}{\beta(\underline{r},t)} \quad . \tag{11}$$

The material energy density is related to the material temperature through equation-of-state tables. This relationship will be expressed as

$$u_m(\underline{r},t) = \gamma(\underline{r},t)\, T(\underline{r},t) \quad , \tag{12}$$

where $\gamma(\underline{r},t)$ will in general depend upon pressure, temperature, etc.

At this point, we assume that the transport equation [Eq. (1)], the energy conservation equation [Eq. (5)], the relation between the material energy density and radiation energy density [Eq. (11)], the relation between the material energy density and the temperature [Eq. (12)], and the miscellaneous definitions that have been given provide an adequate mathematical description of the problem. The proposed method for solving these equations in the absence of scattering is discussed in Sec. III.

*Note that $u_r(\underline{r},t)$ is not the energy density of the radiation field.

III. IMPLICIT MONTE CARLO METHOD IN THE ABSENCE OF SCATTERING

A. Complete Emission Term

The emission source term of the transport equation is evaluated by solving the energy conservation equation [Eq. (5)] for $u_r(\underline{r},t)$. In the absence of scattering, the $u_r(\underline{r},t)$ that satisfied Eq. (5) is given by

$$u_r(\underline{r},t) = \left[u_r(\underline{r},t^o)\, e^{-\int_{t^o}^{t} c\beta\sigma_p dt'} + \int_{t^o}^{t} dt'\beta(\underline{r},t')\, e^{-\int_{t'}^{t} c\beta\sigma_p dt''} \left\{ S(\underline{r},t') + \int\int \mu_a(\nu)\, I(\underline{r},\nu,\underline{\Omega},t')\, d\nu d\underline{\Omega} \right\} \right] , \quad t \geq t_o \quad , \tag{13}$$

where $u_r(\underline{r},t^o)$ is a specified initial condition at t^o.

The solution for $u_r(\underline{r},t)$, as given by Eq. (13), may be utilized in the source term of the transport equation, as given by Eq. (8), to express the transport equation in the absence of scattering as

$$\frac{1}{c}\frac{\partial I(R)}{\partial t} + \underline{\Omega}\cdot\underline{\nabla}\, I(R) + \mu_a(\nu)\, I(R) = \frac{c}{4\pi}\mu_a(\nu)\, b_\nu \left[u_r(\underline{r},t^o)\, e^{-\int_{t^o}^{t} c\beta\sigma_p dt'} + \int_{t^o}^{t} dt'\beta(\underline{r},t')\, e^{-\int_{t'}^{t} c\beta\sigma_p dt''} \left\{ S(\underline{r},t') + \int\int \mu_a(\nu)\, I(\underline{r},\nu,\underline{\Omega},t')\, d\nu d\underline{\Omega} \right\} \right] . \tag{14}$$

The emission source term is now specified in terms of the intensity I, an extraneous heat source S, and an initial condition $u_r(\underline{r},t^o)$. It will subsequently be shown that the integration of the individual source term, which contains the intensity, may be done with Monte Carlo. The time and space dependence of $u_r(\underline{r},t^o)$ and any extraneous heat source are assumed to be known. There is some approximation here, in practice, because $u_r(\underline{r},t^o)$ is usually replaced by its cell average value computed from the previous time step. However, there is an additional complication that affects all three source terms. The quantities μ_a, b_ν, and β are also functions of time since they depend upon the temperature. In general, the time dependence of these quantities is not known and must be extrapolated in some manner from information before $t = t^o$.

The method developed by Fleck and Cummings essentially consists of allowing for an extrapolation of σ_p and β (if necessary), replacing the exponentials in Eq. (14) by their first-order expansions, and using a time-centering parameter (α) in a finite difference approximation. In this report, the time-dependent behavior of σ_p and β will be extrapolated, but the photon source in the Monte Carlo calculation will be sampled directly rather than incorporating the additional approximations of first-order expansions of exponentials and of time centering. Previous calculations have shown that σ_p and β generally, though not always, display a nearly exponential behavior with time and that the product $\sigma_p\beta$ is almost constant. Therefore, the time-dependent behavior of σ_p and β during the time interval will be extrapolated as

$$\sigma_p(\underline{r},t) = \sigma_p(\underline{r},t^o)\, e^{-C_1(t-t^o)/(t^o-t^{-1})} , \quad t^o \leq t \leq t^1 , \tag{15}$$

and

$$\beta(\underline{r},t) = \beta(\underline{r},t^o)\, e^{C_1(t-t^o)/(t^o-t^{-1})} , \quad t^o \leq t \leq t^1 , \tag{16}$$

so that

$$\sigma_p(\underline{r},t)\,\beta(\underline{r},t) = \sigma_p(\underline{r},t^o)\,\beta(\underline{r},t^o) , \quad t^o \leq t \leq t^1 , \tag{17}$$

where t^1 denotes the time at the end of the current time interval and t^{-1} denotes the beginning of the previous time interval. The constant C_1 may be determined from the information at the end of the previous time interval as

$$C_1 = \frac{1}{2} \ln \left[\frac{\sigma_p(\underline{r},t^{-1})\ \beta(\underline{r},t^o)}{\sigma_p(\underline{r},t^o)\ \beta(\underline{r},t^{-1})} \right] \quad , \tag{18}$$

where σ_p and β would generally be cell average quantities in an actual calculation.

In the following subsections, the sampling of the individual terms of the emission source is considered. In all cases, we extrapolate σ_p and β with Eqs. (15) and (16). For the purpose of sampling collision points, the value of the attenuation coefficient at the beginning of the time interval is utilized and similarly $\mu_a(\nu)b_\nu/\sigma_p$ is assumed to be independent of time when sampling for ν.

B. Sampling the $u_r(\underline{r},t^o)$ Source Term

The total photon energy per unit volume produced in a time Δt by the first term on the right-hand side of Eq. (14) is obtained by multiplying this term by $d\underline{\Omega}\ d\nu\ \Delta t$ and integrating over $\underline{\Omega}$ and ν. The result of this operation gives the energy

$$c\ \sigma_p(\underline{r},t^o)\ u_r(\underline{r},t^o)\ e^{-C_2(t-t^o)}\ \Delta t \quad ,$$

$$t^o \leq t \leq t^1 \quad , \tag{19}$$

where C_2 is defined as

$$C_2 = c\ \beta(\underline{r},t^o)\ \sigma_p(\underline{r},t^o) + \frac{C_1}{t^o - t^{-1}} \quad . \tag{20}$$

Therefore, the total energy per unit volume produced by this source term during the time interval is given by D_1 as

$$D_1 = \frac{u_r(\underline{r},t^o)\ c\sigma_p(\underline{r},t^o)}{C_2} \left[1 - e^{-C_2(t^1-t^o)} \right] . \tag{21}$$

The time of a photon birth may be sampled in the Monte Carlo simulation with the density function obtained by dividing Eq. (19) by $D_1\Delta t$. Therefore, the time is sampled as

$$t = t^o - \frac{1}{C_2} \ln \left[1 - \xi \left\{ 1 - e^{-C_2(t^1-t^o)} \right\} \right] \quad , \tag{22}$$

where ξ is a random number on the unit interval.

The total energy produced in a cell during the time interval, assuming cell average quantities to describe $u_r(\underline{r},t^o)$, $\sigma_p(\underline{r},t^o)$, and $\beta(\underline{r},t^o)$, is simply the product of D_1 and the cell volume. This energy is distributed in the Monte Carlo simulation to a number of source particles. The initial time of each of these source particles is selected with Eq. (22), each initial spatial position is selected randomly within the cell, each direction of flight is selected from an isotropic distribution, and each frequency is selected with the density function

$$\mu_a(\nu)\ b_\nu/\sigma_p \quad , \tag{23}$$

which is normally evaluated at t^o although in principle it could also be extrapolated.

C. Sampling the Implicit Source Term

The total energy per unit volume produced in a time Δt by the last source term on the right-hand side of Eq. (14) is obtained by multiplying this term by $d\underline{\Omega}d\nu\Delta t$ and then integrating over $\underline{\Omega}$ and ν. The result of this operation gives the energy

$$c\sigma_p(\underline{r},t^o)\ \beta(\underline{r},t^o)$$

$$\times \int_{t^o}^{t} \left\{ e^{-C_2(t-t')} \int\int \mu_a(\nu')I(\underline{r},\nu',\underline{\Omega}',t')d\nu'\ d\underline{\Omega}' \right\}$$

$$\times\ dt'\Delta t \quad . \tag{24}$$

The integral over ν', $\underline{\Omega}'$, t' will be done with Monte Carlo so that

$$\mu_a(\nu')I(\underline{r},\nu',\underline{\Omega}',t')d^3r d\nu' d\underline{\Omega}' dt' = \sum_i W_i \quad , \tag{25}$$

where W_i is a photon weight and the summation is over all collisions that occur in the phase space volume $d^3r d\nu' d\underline{\Omega}' dt'$. Hence, each collision may be thought of as performing the integration over the prime variables in Eq. (24). The Monte Carlo is also integrating this source term over the cell volume because $\mu_a I$ is the photon energy dumped at collisions per unit volume.

We now focus our attention on the ith collision. The amount of photon energy produced in Δt, due to this collision, may be obtained from Eqs. (24) and (25) as

$$c\sigma_p(\underline{r},t^o)\,\beta(\underline{r},t^o)e^{-C_2(t-t')} W_i\,\Delta t \quad , \quad t \geq t' \quad , \qquad (26)$$

where W_i is the photon weight upon entering the collision and t' is the time of the collision. Therefore, the total energy of the subsequent photons produced in the time interval, as a direct result of this collision, is given by the integral of Eq. (26) over t from t' to t^1. This total energy, defined as D_2, is

$$D_2 = \frac{c\sigma_p(\underline{r},t^o)\,\beta(\underline{r},t^o)}{C_2} W_i \left\{1 - e^{-C_2(t^1-t')}\right\} . \qquad (27)$$

The D_2 energy may be given to an individual photon that begins its life history at the collision point. However, there is a time delay between the time the original photon suffers a collision and the time the new photon is emitted. This time delay is randomly determined with the density function obtained by dividing Eq. (26) by $D_2\Delta t$. The new time is sampled as

$$t = t' - \frac{1}{C_2} \ln\left[1 - \xi\left\{1 - e^{-C_2(t^1-t')}\right\}\right] . \qquad (28)$$

The emerging photon direction of flight is selected from an isotropic distribution and the frequency is selected with the density function

$$\mu_a(\nu)\, b_\nu/\sigma_p \quad . \qquad (29)$$

Allowing the photon to always scatter and adjusting its weight at each collision will produce an undesirable fluctuation of weights. The following pseudoscattering procedure may be used to eliminate this fluctuation of weights.

a. For $D_2/W_i < 1$, a pseudoscattering collision is allowed to occur with probability

$$1 - f = \frac{c\,\sigma_p(\underline{r},t^o)\,\beta(\underline{r},t^o)}{C_2}\left\{1 - e^{-C_2(t^1-t')}\right\} \qquad (30)$$

and the history of the incident photon is continued without altering its weight. With probability f, the history of the incident photon is terminated.

b. For $D_2/W_i > 1$, splitting is utilized to avoid weight multipliers greater than unity. This splitting is accomplished by setting n to the largest integer that is less than or equal to D_2/W_i and this value of n is increased by one with probability $\frac{D_2}{W_i} - n$. The incident photon weight is then split into n different photons, each of which emerge with the weight of the incident photon.

In either of the above cases, the new time after the pseudoscattering collision is selected from Eq. (28), the frequency is selected with the density function of Eq. (29) and the direction of flight is selected isotropically.

The retardation in time at these pseudoscattering collisions arises naturally from the basic physical equations. This results because the material energy gained by photon absorption increases the probability of subsequent photon emission after the absorption event.

D. Sampling the S Source Term

The part of the emission source term in Eq. (14) that is due to the extraneous heat source S depends upon the time-dependent behavior of S. For complicated situations, this term must be tabulated numerically. Here we consider the simple case of

$$S(\underline{r},t) = S_o = \text{constant} \qquad (31)$$

within a cell, which may be simulated without numerical tables.

The total energy per unit volume produced by this source term in a time Δt is given by

$$\frac{c\,\sigma_p(\underline{r},t^o)\,\beta(\underline{r},t^o)}{C_2}\,S_c\left[1-e^{-C_2(t-t^o)}\right]\Delta t \quad ,$$

$$t^o \le t \le t^1 \quad . \tag{32}$$

Hence, the total photon energy per unit volume produced by this term during the time interval is given by

$$D_3 = \frac{c\,\sigma_p(\underline{r},t^o)\,\beta(\underline{r},t^o)\,S_o}{C_2}$$

$$\times\left\{t^1 - t^o - \frac{1}{C_2}\left[1-e^{-C_2(t^1-t^o)}\right]\right\} \quad . \tag{33}$$

A rejection scheme for sampling the initial photon time from the density function is given in Fig. 1. The efficiency of this scheme increases monotonically from 1/2 for $|C_2(t^1 - t^o)| \sim 0$ to 1 for $|C_2(t^1 - t^o)| \to \infty$. Here, efficiency is defined as the probability of success per trial.

The selection of the initial space coordinates, the direction of flight, and the frequency of the photon are identical to the corresponding selection for the u_r term.

E. Energy Balance at the End of a Time Step

The relation between the material energy density and the radiation energy density as given by Eq. (11) may be utilized to write Eq. (5) in the form

$$\frac{\partial u_m(\underline{r},t)}{\partial t} = \left[\int\int \mu_a(\nu)\,I(R)d\nu\,d\underline{\Omega}\right]$$

$$-c\,\sigma_p(\underline{r},t)\,u_r(\underline{r},t) + S(\underline{r},t) \quad , \tag{34}$$

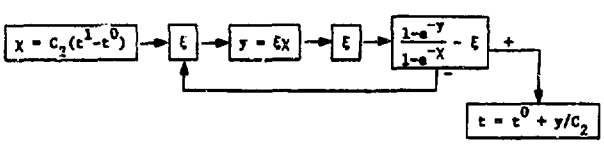

Fig. 1. Selection of t for the S source term.

where real scattering is still being neglected. This equation is multiplied by $d^3rdt/\Delta V$ and integrated over a cell volume and a time interval to obtain

$$\overline{u_m(t^1)} - \overline{u_m(t^o)} = \left\{\left[\begin{array}{l}\text{Total photon energy lost at col-}\\ \text{lisions within the cell during}\\ \text{the time interval.}\end{array}\right]\right.$$

$$-\left[\begin{array}{l}\text{Total photon energy created within}\\ \text{the cell during the time interval}\end{array}\right]$$

$$\left.+\left[\begin{array}{l}\text{Extraneous heat introduced into the}\\ \text{cell during the time interval.}\end{array}\right]\right\}/\Delta V, \tag{35}$$

where the bars denote an average over the cell and ΔV is the volume of the cell. The first and second terms on the right-hand side of Eq. (35) are obtained from the Monte Carlo calculation during the time interval. Since $\overline{u_m(t^o)}$ and the extraneous source term are assumed to be known quantities, $\overline{u_m(t^1)}$ may be determined from Eq. (35).

In the case of a perfect gas, the average temperature within the cell at the end of the time step is computed as

$$\overline{T(t^1)} = \overline{u_m(t^1)}/\gamma \quad , \tag{36}$$

where γ is a constant. In the more general situation, γ is not a constant so that Eq. (36) would be determined by iteration with γ obtained from equation-of-state tables. In either case, the radiation cell-averaged energy density is

$$\overline{u_r(t^1)} = a\overline{[T(t^1)]}^4 \quad . \tag{37}$$

F. Summary of the Monte Carlo Calculation in the Absence of Scattering

A typical Monte Carlo calculation that uses the sampling scheme described in this section is summarized to clarify the sampling procedure and to provide a convenient reference for comparisons with other schemes such as that previously proposed by Fleck and Cummings. The calculation will be described for a time step beginning at t^o and continuing to t^1. We assume that initial information at t^o is available from the previous time step. This would include a temperature, a material energy density, a radiation energy density, cross sections,

and other necessary data for each cell. There would also be a source of photons that consists of those photons that reached the time boundary t^o during the last time-step calculation.

The derivation in this section has been presented for one given cell so that all quantities should have a cell subscript. This cell identifier will be denoted here by a j. The following computational steps are for the time interval from t^o to t^1.

1. Make necessary adjustments in the photon source* that consists of those photons that reached the time boundary t^o during the last time step. This may, for example, include a combing method to equalize photon weights and to increase or decrease the number of such photons by properly adjusting photon weights.

2. Create an additional source of photons that initially carry a total photon energy $D_{1j}\Delta V_j$ in each cell. Here, D_{1j} is determined from Eq. (21) along with volume average values of u_{rj}, σ_{pj}, and C_{2j}. The initial coordinates of each photon are sampled as discussed in part B of this section; i.e., t from Eq. (22), the direction of flight isotropically, ν from $\mu_a(\nu)b_{\nu j}/\sigma_{pj}$, and the space coordinate randomly within the cell.

3. Create an additional source of photons due to the S source term if nonzero, as discussed in part D, and also create photons from any extraneous photon sources that may be present.

4. For each photon of steps 1, 2, and 3, sample its subsequent history and the history of its progeny (due to pseudoscattering events) until absorption, leakage, or time termination at t^1 occurs. At each collision, sample for a pseudoscattering event as discussed in part C, i.e., follow steps (a) and (b) on p. 5 to decide if pseudoscattering occurs. If not, terminate the history. Otherwise, sample the new time from Eq. (28), sample the new frequency from the density function $\mu_a(\nu)\, b_\nu/\sigma_{pj}$, sample the direction of flight isotropically, and proceed with the weight that the photon had before the collision (in the case of step (b) on p. 5, more than one photon may emerge from the collision point).

5. Tabulate the total photon energy lost at collision events and the total photon energy created at pseudoscattering events for subsequent use in an energy balance at the end of the Monte Carlo. Rather than doing this at collisions, there are statistical advantages obtained for optically thi cells by using a path length estimator. Thus for ea flight path

$$\text{Energy lost to collision events} = \mu_a(\nu)\, sW \quad , \tag{38}$$

$$\text{Energy created due to pseudoscattering events} = \mu_a(\nu) \int_o^s D_2 ds'$$

$$= \mu_a(\nu) \int_{t'-s/c}^{t'} D_2 c\, dt$$

$$= \mu_a(\nu)\, \frac{s\, W\, c\, \sigma_{pj}\, \beta_j}{C_{2j}}$$

$$\times \left\{1 - \frac{c}{C_{2j}s}\left[e^{-C_{2j}(t^1-t')} - e^{-C_{2j}(t^1-t'+\frac{s}{c})}\right]\right\} \quad , \tag{39}$$

where s is the length of the flight path that originates at $t = t' - s/c$ and terminates at $t = t'$. Here, W is the photon weight and the flight path is defined to be terminated (for scoring purposes) whenever the photon suffers a collision, reaches a cell boundary, or reaches time cut-off. Note that this path length scoring does not affect the sampling at pseudoscattering collisions. However, it is important to observe that for a flight path terminating with a collision, the exponential $e^{-C_{2j}(t^1-t')}$ also appears in Eqs. (27) and (28). Hence, this exponential should only be evaluated on the machine once for each collision.

6. After all photons are processed in step 4, compute the new material energy density in each cell from Eq. (35). The cell temperatures are computed with Eq. (36), by iteration if necessary. Then the average radiation energy density for each cell is obtained from Eq. (37). The other necessary data, such as cross sections, that will be needed for the next time step are computed by utilizing the average cell temperatures at t^1.

7. Return to step (1) for the next step.

*The word photon will be used here to denote a bundle of photon energy.

This method may be compared to the method suggested by Fleck and Cummings. The methods are similar in the limit of a small time step although the method proposed here does have a time delay at pseudoscattering events even for small time steps. The method here suffers from the disadvantage that one exponential and one logarithm must be evaluated at each pseudoscattering event. However, the advantage gained by treating the time-dependent behavior in a more exact manner should allow longer time steps and hence more than counteract this disadvantage.

G. Elimination of Pseudoscattering Domination

The implicit approach is used to improve accuracy and to incorporate stability in the calculations. However, it has certain difficulties that are not encountered in a purely explicit calculation. For example, if the quantity f is nearly zero for the majority of the collisions within a cell and if the cell is many mean free paths thick, a photon may suffer a large number of pseudocollisions before being terminated by absorption. This is a physically possible situation in many problems since cells tend to be very thick at low temperatures (thousands or even millions of mean free paths) and since f tends to be near zero for cells where the temperature is changing slowly. It is instructive that this type of problem also occurs in the scheme of Fleck and Cummings and seems to be an inherent property of the implicit method of solution. In their scheme, the quantity f may be increased by properly setting the time-centering parameter α.

For cells and time intervals where multiscatterings are a problem (these could be identified, for example, as cells where the product of σ_p with a typical cell dimension is greater than 20 and that also satisfy the criterion that $f < 0.05$ at the beginning of the time interval), the following partially explicit approach could be used. The source term in the transport equation is written as

$$(1-p)\,\frac{c}{4\pi}\,\mu_a(\nu)\,b_\nu\,u_r(\underline{r},t^o) + p\,X \quad \text{(source term in Eq. (14))}, \tag{40}$$

where p is an input probability for each cell so that $0 \leq p \leq 1$. Then all energy sources in the previous derivation of this section, including the pseudoscattering source, are multiplied by p. Also, there is an additional explicit source with a photon energy per unit volume of

$$D_4 = (1-p)\,c\,\sigma_p(\underline{r},t^o)\,u_r(\underline{r},t^o)(t^1 - t^o) \ . \tag{41}$$

The initial photon time for this source is selected as

$$t = t^o + (t^1 - t^o)\xi \quad , \tag{42}$$

the direction of flight is selected isotropically, and ν is selected with the density function $\mu_a(\nu)\,b_\nu/\sigma_p$. Here again σ_p and u_r would generally represent cell-averaged quantities.

This method has the advantage that a certain amount of mathematical rigor is preserved whereas for cells where multiscattering events are a problem, the probability p may be set so as to reduce the number of scattering events to an acceptable level. For example, for such cells p could be set so that the pseudoscattering probability is 0.95 at the beginning of the time step. This criterion for p may be inserted into Eq. (30) to yield

$$p = \frac{0.95\,c_2}{c\sigma_p(\underline{r},t^o)\,\beta(\underline{r},t^o)\left[1 - e^{-c_2(t^1-t^o)}\right]} \ . \tag{43}$$

It seems advisable to use a ($p \neq 1$) only when absolutely necessary because the implicit approach has stability advantages over the explicit approach. It should also be noted that $\sigma_p\,u_r$ in Eq. (41) could be extrapolated in some manner. We did not extrapolate here because we anticipated that this semiexplicit approach would be needed in low-temperature regions where statistics are already poor. This makes the validity of an extrapolation highly questionable.

H. Comments on Cell Averaging

Both the method proposed in this section and the method of Fleck and Cummings suffer from the limitation that a number of space-dependent quantities must be repaced by cell averages. There isn't much one can do about this limitation with the one

exception of the space dependence of the $u_r(\underline{r},t^o)$ source term within a cell. In the method proposed in this section, we have used this initial condition for only one time interval. It is possible to use the same initial condition for a number of subsequent time intervals so that the source term due to collisions in the Monte Carlo calculation becomes the dominant term after the initial condition term has died out. The spatial position in the implicit term is simply the position of the collision and represents no additional difficulty with cell averages. We explore this method in Appendix A.

IV. EXAMPLE PROBLEMS

A. Introduction

The implicit Monte Carlo method of Sec. III was used to solve two slab geometry problems. The apportionment of source photons and the computation of cycle time widths was similar in the two problems. These similarities will be discussed before considering the results of the individual calculations.

Both problems were driven by a blackbody source of photons positioned on the left surface of a slab. This blackbody source was held at a fixed temperature for the duration of the calculation. In the Monte Carlo simulation, initial photon coordinates were sampled from three separate sources at the beginning of each time step. These sources included the blackbody surface source, the explicit source term of Sec. III.B, and the explicit source term (if nonzero) in Sec. III.G. The total photon weight (energy) due to each of these three sources is a known quantity at the beginning of a time step. The code distributed this total energy to the source photons in such a manner that each photon began its life history in the time cycle with approximately the same weight. The number of photons to be started from each of the three sources was computed so that the total number of photons in the photon bank at the beginning of a time step was approximately equal to an input constant. This total number of photons in the bank at the beginning of a time step is equal to the sum of the number sampled from the three sources plus those photons that remain from the previous time step.

The widths of the cycle time steps were allowed to change in the course of each calculation. A time-step width was computed on the basis of the maximum fractional material energy density change (δ) that occurred for any cell during the previous time step, so that

$$\Delta t_{new} = \left(\frac{\varepsilon}{\delta}\right) \Delta t_{old} \quad . \tag{44}$$

That is, the time step width is extrapolated to yield an expected maximum fractional material energy density change of ε. ε was an input parameter for each calculation. In addition, it was required that $\Delta t_{min} \leq \Delta t \leq \Delta t_{max}$, where Δt_{min} and Δt_{max} are also input for each calculation.

B. Example Problem with Constant ($\beta\sigma_p$)

The first example problem was also used by Fleck and Cummings.[1] A 4-cm-thick slab is heated by a 1-keV blackbody photon source on the left face of the slab. The macroscopic cross section is specified by the simple expression

$$\mu_a(\nu) = \frac{27}{\nu^3}\left(1 - e^{-\nu/T}\right) \text{ cm}^{-1} \quad , \tag{45}$$

where ν and T are measured in units of keV. The temperature in all cells is initially set to 0.001 keV to keep σ_p finite. A perfect gas model is used with γ specified to be 0.008118 jerks/keV/cm^3. Using the perfect gas model also implies that β is proportional to the cube of the material temperature,

$$\beta(\underline{r},t) = \frac{4a}{\gamma} T(\underline{r},t)^3 \quad . \tag{46}$$

Because $\sigma_p(\underline{r},t)$ is inversely proportional to the cube of the temperature for the cross section of Eq. (45), the product ($\beta\sigma_p$) is independent of the material temperature. Therefore, the extrapolation of ($\beta\sigma_p$) with Eq. (17) is exact for this problem even though the extrapolation of β or σ_p separately is not exact.

We found that the extrapolation of β and σ_p, based on the C_1 value obtained with Eq. (18), tends to "overshoot" since the extrapolation is based on only the preceding time step. Therefore, for the calculations presented here, the extrapolation of C_1 was based on a quadratic fit of the previous two time steps.

The results of the implicit Monte Carlo calculation for various time-step control values of ε are given in Fig. 2. In these calculations, cell widths of 0.4 cm were utilized and the total number of photons at the beginning of each time step was held at approximately 24,000. The computed temperatures are nearly independent of ε from t = 0 to t = 0.05 sh since the input time-step minimum of 0.002 sh is greater than the time-step width computed with Eq. (44). For t > 0.05 sh, the larger ε calculations use larger time steps, but there seems to be little difference in overall accuracy.

The curves shown in Fig. 2 at t = 0.4 sh are typical of the results at equilibrium. The cell temperatures exhibit significant fluctuations from time step to time step that are somewhat similar to the fluctuations observed in Fig. 2 with different values of ε. However, the computed material energy of the entire slab is relatively stable between subsequent time steps with a standard deviation of about 1.3%.

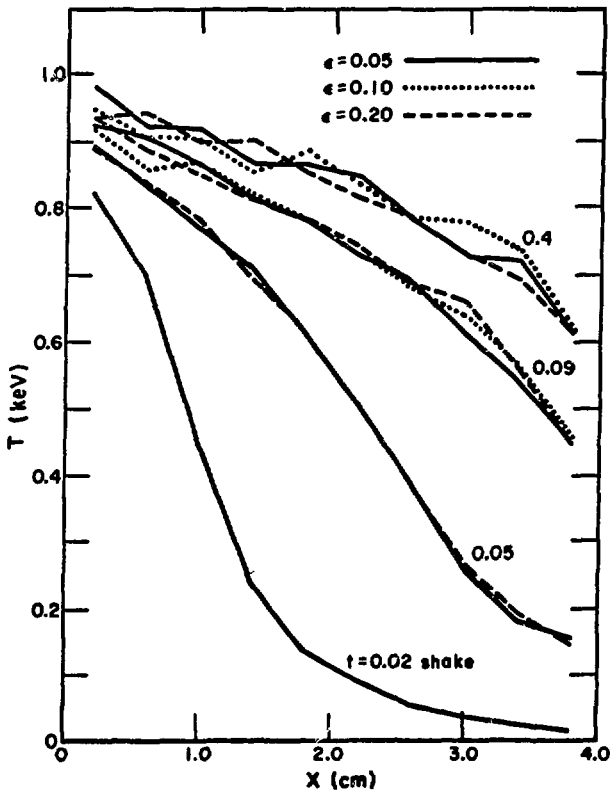

Fig. 2. Temperature of slab heated by a 1-keV blackbody photon source at x = 0.

In the calculations of Fig. 2, the path-length estimator of Eqs. (38) and (39) was used for energy deposition. This results in typical statistical energy balance errors of from 1 to 3% relative to the total material energy in the slab. Some calculations have also been made with a collision estimator, which conserves energy exactly. The results indicated that, for a fixed amount of machine time, the path-length estimator seems to yield statistically better temperatures at near-equilibrium conditions. However, it is difficult to draw conclusions without comparing ensembles of such calculations.

The calculations reported in Fig. 2 used a cross section and perfect gas model such that the product $(\beta\sigma_p)$ was independent of temperature. We turn now to a more challenging problem where the product $(\beta\sigma_p)$ also depends upon the temperature.

C. Example Problem with $(\sigma_p\beta) \sim 1/\sqrt{T}$

The cross section for this calculation was given by

$$\mu_a(\nu) = \frac{970.99}{\sqrt{T}\,\nu^3}\ \text{cm}^{-1} \tag{47}$$

with ν and T measured in units of keV. This is approximately the cross section of iron for ν and T in the low keV range where inverse Bremsstrahlung is dominant. The cross section of Eq. (47) results in a σ_p of

$$\sigma_p(\underline{r},t) = \frac{149.52}{[T]^{7/2}}\ \text{cm}^{-1} \quad . \tag{48}$$

The perfect gas model was again used with a γ of 0.03820 jerks/cm^3/keV. Thus, the product $\beta\sigma_p$ is inversely proportional to the square root of the temperature.

The photon source on the left face of the slab was a 2-keV blackbody source for the duration of the calculation. All photons reaching the boundary on the left face of the slab were reflected back. All photons reaching the boundary on the right face were allowed to escape from the system. Ten equal mesh intervals were again used across a 4-cm-thick slab.

The result of an implicit calculation with an ε time-step control value of 0.05 are given in Fig. 3. The total number of photons at the beginning of

each time step in this calculation was held at approximately 24,000. The temperatures tend to vary smoothly during the initial temperature rise, but some fluctuation is observed at near-equilibrium conditions as may be seen from the last two time curves of Fig. 3. However, the overall results are satisfying because the minimum time-step width used here, Δt min, is 0.0005 sh. This time-step width is about a factor of 10^3 greater than the time-step width where a pure explicit calculation becomes unstable.

This calculation was repeated allowing only about 6000 photons in the bank at the beginning of each time step. The results agreed with the 24,000 photon calculation, although statistical fluctuations were somewhat greater.

In the initial calculations on this problem, we found that a path-length estimator produced unacceptable instabilities at low temperatures. Therefore, in the calculations reported here, a collision estimator was used for flight paths such that the number of mean free paths across a cell was greater than 20. Otherwise, a path-length estimator was used.

The initial conditions of this problem were changed for one test calculation to observe the application of the implicit method for decreasing temperatures. All cells were specified to have an initial temperature of 20 keV without any photons present. Then the resulting temperature as a function of time was observed with reflecting boundary conditions specified on each side of the slab. The temperature decayed until a near-equilibrium condition was reached so that the photon field was approximately in equilibrium with the material. No difficulties were encountered, and the temperature distribution remained flat across the slab (except for statistical fluctuations) as expected.

V. IMPLICIT MONTE CARLO METHOD WITH SCATTERING

A. Complete Emission Term

In this section, real scattering is included so that the transport equation is

$$\frac{1}{c}\frac{\partial I(R)}{\partial t} + \underline{\Omega}\cdot\underline{\nabla} I(R) + \mu_t(\nu)\, I(R) = \frac{c}{4\pi}\mu_a(\nu)\, b_\nu \left(u_r(\underline{r},t^o)\, e^{-\int_{t^o}^{t} c\beta\sigma_p dt'} + \int_{t^o}^{t} dt'\, \beta(\underline{r},t')\, e^{-\int_{t'}^{t} c\beta\sigma_p dt''} \right.$$

$$\left. \times \left\{ S(\underline{r},t') + \int\int I(\underline{r},\nu,\underline{\Omega},t') \left[\mu_t(\nu) - \int\int \frac{\nu'}{\nu}\, \mu_s(\nu\to\nu',\underline{\Omega}\cdot\underline{\Omega}')\, d\nu'\, d\underline{\Omega}' \right] d\nu\, d\underline{\Omega} \right\} \right)$$

$$+ \int\int \frac{\nu}{\nu'}\, \mu_s(\nu'\to\nu,\underline{\Omega}\cdot\underline{\Omega}')\, I(\underline{r},\nu',\underline{\Omega}',t)\, d\nu'\, d\underline{\Omega}' \quad . \tag{49}$$

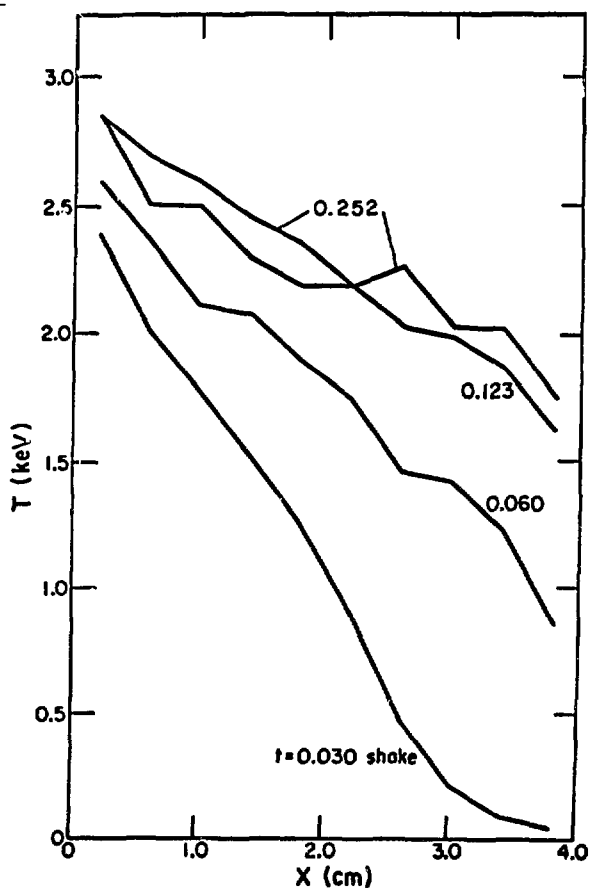

Fig. 3. Temperature of slab heated by a 2-keV blackbody photon source at x = 0.

The $u_r(\underline{r},t^o)$ term and the $S(r,t')$ term have not changed from the treatment discussed in Sec. III so they will not be repeated here. However, the implicit source term has changed so we will consider it.

B. Implicit Source Term

The extrapolation of σ_p and β is still assumed to be given by Eqs. (15) and (16) of Sec. III. The total energy emerging from a collision (real scattered plus pseudoscattered) is given by

$$D_2 = \frac{c\,\sigma_p(\underline{r},t^o)\,\beta(\underline{r},t^o)}{C_2}\,W_i\left[1 - e^{-C_2(t^1-t')}\right]$$

$$\times\left[1 - \frac{1}{\mu_t(\nu')}\int\int\frac{\nu''}{\nu'}\,\mu_s(\nu'\to\nu'',\underline{\Omega}'\cdot\underline{\Omega}'')d\nu''d\underline{\Omega}''\right]$$

$$+ W_i\,\frac{1}{\mu_t(\nu')}\int\int\frac{\nu''}{\nu'}\,\mu_s(\nu'\to\nu'',\underline{\Omega}'\cdot\underline{\Omega}'')d\nu''d\underline{\Omega}'', \quad (50)$$

where the photon coordinates upon entering the collision are designated to be $r,\nu',\underline{\Omega}',t'$. The last term on the right-hand side of Eq. (50) is identified as a real scattering term while the remainder is a portion of the photon source due to emission.

A number of interesting observations may be made for various scattering interactions. We first note that when $\mu_s = 0$, Eq. (50) reduces to Eq. (27) in Sec. III with pure absorption. Another interesting case occurs when all scattering is coherent. Then the right-hand bracket of the first term on the right-hand side of Eq. (50) becomes $\mu_a(\nu')/\mu_t(\nu')$. This means that coherent scattering does not contribute to the emission term in agreement with energy conservation. A scattering kernel where all photons suffering a real scattering collision will lose energy is another case of interest. Then the emission term becomes greater than for the corresponding case of pure coherent scattering. This makes sense physically since the real scattering is feeding energy to the material. Finally, one may consider a scattering kernel so that the majority of the radiation gains energy at a collision. Then the emission term in Eq. (50) becomes negative because the scattering of radiation is taking energy from the material. This type of scattering, which will be discussed later, introduces certain problems in the Monte Carlo.

The last term on the right-hand side of Eq. (50) may be treated with an analog scattering method. A real scattering is allowed to occur with probability $\mu_s(\nu')/\mu_t(\nu')$, where

$$\mu_s(\nu') = \int\int\mu_s(\nu'\to\nu'',\underline{\Omega}'\cdot\underline{\Omega}'')d\nu''d\underline{\Omega}'' \quad . \quad (51)$$

For a real scattering event, the new energy and direction of flight are selected with the kernel $\mu_s(\nu'\to\nu'',\underline{\Omega}'\cdot\underline{\Omega}'')$ and the final photon weight is multiplied by the factor ν''/ν'.

Irrespective of the result of sampling for the real scattering, the first term on the right-hand side of Eq. (50) must also be treated at each collision. For the method described here, we let A be the value of this term and first consider the case when A is greater than zero. Then if A/W_i is less than unity, a pseudoscattering is allowed to occur with probability A/W_i. If A/W_i is greater than unity, we set n to the largest integer that is less than or equal to A/W_i, increase n by one with probability $(A/W_i)-n$, and allow n photons to emerge from the collision. For such pseudoscattering events, the new time is selected from Eq. (28), the direction of flight is selected from an isotropic distribution, and the frequency is selected from the density function $\mu_a(\nu)b_\nu/\sigma_p$. These photons, which suffer a pseudoscattering event, emerge from the collision point with the incoming photon weight W_i.

For scattering kernels where A may be less than zero, the situation is more complicated. Of course, one could allow negative weights, but this tends to increase statistical errors. There are at least two alternatives that appear practical. The first alternative is discussed by Fleck[2] and involves absorbing the loss term in Eq. (50) into the S term as evaluated at t^o. Because this approach has already been discussed by Fleck, we consider a second alternative, which is to tabulate a quantity that we call Q for each cell. Then whenever a collision occurs where A is negative, Q is changed as

$$Q = (Q)_{old} + A \quad . \quad (52)$$

However, if a collision occurs with a positive A, the value of Q for the cell is checked. For a Q

of zero, the emitted photons are sampled as discussed before for positive A. For a Q less than zero but such that $|Q| > A$, Q is increased as

$$Q = (Q)_{old} + A \qquad (53)$$

and the history of the photon is terminated. For a Q less than zero but such that $|Q| < A$, Q is set to zero, A is reduced by the old value of Q, and the emitted photons are sampled as discussed before for this new positive value of A.

This procedure is approximate in the sense that the spatial position within the cell and the time of the collision are ignored for tabulating Q. The procedure also may result in Q values at the end of the time interval that are nonzero. Such Q values should be added to the $u_r(\underline{r},t^o)$ source term for the next time cycle; i.e., the $u_r(\underline{r},t^o)$ source term is reduced.

The inclusion of scattering in the implicit Monte Carlo requires sampling the scattering kernel for a new photon energy and direction of flight at real scattering events. This sampling is straightforward for Thompson scattering and there are also numerous schemes proposed for sampling from the Klein-Nishina differential cross section. For the so-called inverse Compton scattering event, where the electron velocity is not negligible so that the photon may actually gain energy at a collision, sampling techniques are not so well developed. In the next section, a Monte Carlo simulation of inverse Compton scattering is discussed.

VI. SAMPLING INVERSE COMPTON SCATTERING EVENTS

A. Introduction

The selection of an emerging photon energy from the Klein-Nishina differential cross section may be accomplished with a variety of well-known techniques. The method suggested in Appendix B utilizes a fairly efficient rejection technique for incident photon energies that are less than three times the rest mass of an electron, but samples directly without rejection for the photon energies greater than three times the rest mass of an electron. The computer time required for this method is not much greater (perhaps as much as 25% for some photon energies) than that required by schemes that sample an approximate inverse function.

The selection of an emerging photon energy, after a Compton scattering, becomes much more difficult when the electron velocities are large enough in magnitude so that they cannot be neglected. Not only does the selection of the emerging photon energy become more complicated, but also the sampling of the scattering angle then depends upon the velocity of the electron.

In the sampling scheme developed here, the electrons are assumed to have a relativistic Maxwellian distribution of velocities at some temperature T. The velocity of the electron that scatters the photon is selected with a rejection technique. A Lorentz transformation of the incident photon energy is then made to the rest frame of the electron, the emerging photon energy and scattering angle in the electron rest frame is selected from the Klein-Nishina differential cross section, and a Lorentz transformation is made back to the laboratory frame to compute the final photon energy and scattering angle in the laboratory frame. The Lorentz transformations do not require a great deal of computation time because only a transformation of the energy and scattering angle is required.

The Compton scattering law for a relativistic Maxwellian distribution of electron velocities is discussed in part B of this section. A method to sample from this scattering law is proposed in part C and a description of a subroutine that does this sampling is given in part D.

B. Discussion of the Scattering Law

The Klein-Nishina differential cross section for a Compton scattering from a free electron is valid in the rest frame of the electron. The corresponding macroscopic Compton cross section in the laboratory frame, when the electrons are in motion is given by [4,5]

$$\mu_s(\nu\to\nu',\underline{\Omega}\to\underline{\Omega}') = \frac{D}{D'}\,\mu_{se}(\nu_e\to\nu_e',\underline{\Omega}_e\to\underline{\Omega}_e') \quad , \qquad (54)$$

where

$\underline{\Omega}$ is the photon direction of flight,

ν is the photon frequency,

$$D = 1 - \underline{\Omega}\cdot\underline{v}/c \quad , \tag{55}$$

$$D' = 1 - \underline{\Omega}'\cdot\underline{v}/c \quad , \tag{56}$$

$\underline{v}$ is the electron velocity in the laboratory system,

$$\lambda = \left[1 - (v/c)^2\right]^{-1/2} \quad , \tag{57}$$

and μ_{se} is the macroscopic Klein-Nishina cross section in the rest frame of the electron. The subscripts e on ν and $\underline{\Omega}$ also denote their observed values as seen from the rest frame of the electron.

The total scattering cross section may be obtained by multiplying Eq. (54) by $d\nu'\, d\underline{\Omega}'$ and integrating over ν', $\underline{\Omega}'$. Since $d\nu'\, d\underline{\Omega}' = \lambda D' d\nu_e'\, d\underline{\Omega}_e'$,[4] the resulting cross section is

$$\mu_s(\nu,\underline{\Omega}) = \int\int \lambda\, D\, \mu_{se}(\nu_e \to \nu_e', \underline{\Omega}_e \to \underline{\Omega}_e')\, d\nu_e'\, d\underline{\Omega}_e'$$

$$= \lambda\, D\, \mu_{se}(\nu_e, \underline{\Omega}_e) \quad , \tag{58}$$

where the absence of arrows denotes an integration over the respective primed coordinate. The result of Eq. (58) could also be obtained by using an invariant transformation for total cross sections.[4,5]

The cross section in Eq. (58) is due to electrons traveling with a velocity $\underline{v}$. The cross section due to a distribution of electron velocities is obtained by multiplying Eq. (58) by the probability that an electron will be traveling in a direction that is within $d\underline{v}$ about $\underline{v}$ and integrating the resulting expression over $\underline{v}$. Thus we write the macroscopic cross section, $\mu_s(\nu,\underline{\Omega})$, due to a distribution of electron velocities as

$$\mu_s(\nu,\underline{\Omega}) = \int \lambda\, D\, \mu_{se}(\nu_e, \underline{\Omega}_e)\, g(\underline{v})\, d\underline{v} \quad , \tag{59}$$

where $g(\underline{v})$ describes the distribution of electron velocities in the laboratory frame. For the considerations here, we will assume that $g(\underline{v})$ is an isotropic relativistic Maxwellian distribution. Hence, we write $g(\underline{v})$ as

$$g(\underline{v})d\underline{v} = f(v)\, v^2\, dv d\underline{\Omega}_v \quad , \tag{60}$$

where

$$f(v) = \frac{m_o\, \lambda^5\, e^{-m_o c^2 \lambda/kT}}{4\pi ckT\, K_2(m_o c^2/kT)} \quad , \tag{61}$$

m_o is the rest mass of the electron, T is the average electron temperature, and $K_2(Z)$ is the modified Bessel function of the second kind of order two. f(v) is normalized so that

$$4\pi \int_o^c f(v) v^2 dv = 1 \quad . \tag{62}$$

If we now define the polar angle of $\underline{\Omega}_v$ to be the cosine of the angle between $\underline{\Omega}$ and $\underline{v}$,

$$\mu_v = \underline{\Omega}_v\cdot\underline{\Omega} \quad , \tag{63}$$

the corresponding integration over the azimuth angle in Eq. (59) may be readily performed. Therefore, the Compton cross section is given by

$$\mu_s(\nu,\underline{\Omega}) = \int_{-1}^{1}\int_o^c \lambda\left(1 - \mu_v \frac{v}{c}\right) \mu_{se}(\nu_e, \underline{\Omega}_e)$$

$$\times\, 2\pi v^2\, f(v) dv d\mu_v \quad , \tag{64}$$

where the Lorentz transformation gives the following relation between ν_e and ν[4],

$$\nu_e = \lambda\nu\left(1 - \mu_v \frac{v}{c}\right) \quad . \tag{65}$$

C. Sampling from the Scattering Law

It is apparent, from Eq. (64) and the considerations which led to Eq. (59), that one could sample the emerging photon energy $\underline{\Omega}'$ and frequency ν' in the laboratory system with the following steps.

(a) Sample an electron velocity v and polar angle μ_v with respect to the incident beam with the two-dimensional density function

$$h(\mu_v, v) = \frac{\lambda\left(1 - \mu_v \frac{v}{c}\right) \mu_{se}\left(\nu_e, \underline{\Omega}_e\right)\, 2\pi v^2\, f(v)}{\mu_s(\nu,\underline{\Omega})} \quad . \tag{66}$$

(b) Compute ν_e from Eq. (65) for the v and μ_v sampled in step (a).

(c) Sample ν_e' and $\underline{\Omega}_e'$ from the Klein-Nishina cross-section $\lambda\mu_{se}(\nu_e \to \nu_e', \underline{\Omega}_e \to \underline{\Omega}_e')$.

(d) Transform back to the laboratory system as discussed in Appendix C.

The previous scheme requires that one sample μ_v and v from the two-dimensional density function of Eq. (66). This appears impractical due to the presence of μ_{se} in the density function. One may therefore replace step (a) of the previous scheme with the following procedure.

(a) Sample v from the density function $4\pi v^2 f(v)$.

(a') Given the v of step (a), sample μ_v from the density function $(1 - \mu_v \frac{v}{c})/2$; $-1 \leq \mu_v \leq 1$.

(a'') Accept the pair μ_v,v with probability

$$\frac{\lambda\mu_{se}(\nu_e, \underline{\Omega}_e)}{[\lambda\mu_{se}(\nu_e, \underline{\Omega}_e)]_{max}} ,$$

where the numerator is evaluated at the μ_v,v selected and the denominator is the maximum value that the numerator may assume. If the pair is not accepted, return to step (a).

This scheme is equivalent to sampling from $h(\mu_v, v)$ of Eq. (66) since

$$\left\{\begin{array}{l}\text{Probability of accepting}\\ \text{a v in dv about v and}\\ \text{a } \mu_v \text{ in } d\mu_v \text{ about } \mu_v\end{array}\right\} \sim \left\{\begin{array}{l}\text{Probability of sam-}\\ \text{pling a v in dv about}\\ \text{v}\end{array}\right\}$$

$$\times \left\{\begin{array}{l}\text{Probability of sampling a } \mu_v\\ \text{in } d\mu_v \text{ about } \mu_v\end{array}\right\}$$

$$\times \left\{\begin{array}{l}\text{Probability of accepting the}\\ \mu_v, \text{v pair}\end{array}\right\}$$

$$= \left\{4\pi v^2 f(v)dv \left(1 - \mu_v \frac{v}{c}\right) \frac{d\mu_v}{2}\right\} \frac{\lambda\mu_{se}(\nu_e, \underline{\Omega}_e)}{\left[\lambda\mu_{se}(\nu_e, \underline{\Omega}_e)\right]_{max}} .$$

It should be noted that $\lambda\mu_{se}(\nu_e, \underline{\Omega}_e)$ is just proportional to the Klein-Nishina microscopic cross section since the electron density in the rest frame multiplied by λ is the electron density in the laboratory system, which is assumed to be constant. Because the Klein-Nishina cross section decreases monotonically with increasing ν_e, the maximum value of $\lambda\mu_{se}(\nu_e, \underline{\Omega}_e)$ occurs at the minimum ν_e; that is, from Eq. (65) the minimum ν_e is zero corresponding to $\mu_v = 1$ and $\frac{v}{c} = 1$.

The efficiency of such a scheme was found to be nearly independent of the electron temperature, but depends markedly on the incident photon energy. The efficiency curve in Fig. 4 was obtained for an electron temperature of 0.2 electron rest mass units. The majority of the collisions generally occur near the left edge of this graph (say less than 0.2), therefore the overall sampling efficiency may lie around 75%. If problems become important with higher photon energies, it will be worthwhile to devise a more efficient scheme for large photon energies.

D. Description of Subroutine Comet

A subroutine has been written to utilize the previously discussed sampling method. This subroutine has been written specifically for the MCG code, but because it is self-contained it may also be useful in other codes for either production runs or as a cross check against other codes.

The technique used to sample v from the density function $4\pi v^2 f(v)$ is discussed in Appendix D. The tables required for this sampling method are constructed with a CALL COMET (-1) statement before the Monte Carlo sampling begins.

A photon energy (ENW1) and the cosine of the scattering angle (ANEW) in the laboratory system are sampled with a CALL COMET (0) statement. The electron temperature at the collision point (TELC) and the incident photon energy in the laboratory system (EOD1) are the only information required by the subroutine. These are made available to the subroutine through a labeled common block, CTN1. All energies

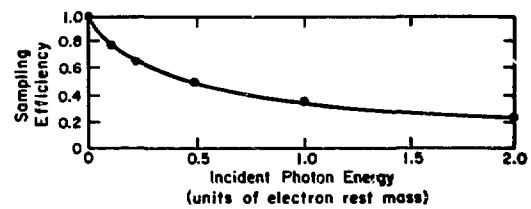

Fig. 4. Monte Carlo sampling efficiency vs incident photon energy at an electron temperature of 0.2.

are in units of the rest mass of an electron. A representative CDC-7600 computation time required by COMET is about 120 μsec for an incident photon of energy 40 keV.

The subroutine will also compute the ratio of the laboratory cross section, due to Maxwellian electrons at a temperature (TELC), to the corresponding Klein-Nishina cross section neglecting electron motion; i.e., at a temperature of zero. This is obtained with a CALL COMET (1) statement, where (TELC) is the temperature and (EOD1) is the photon energy in the laboratory system. The subroutine returns the cross section ratio (CMTCS) and the average relative energy gain (PECA), or loss, of the photon in a Compton collision. The variable PECA is defined as ΔE/EOD1, where ΔE is the average energy gain, or loss, in a Compton collision for an incident photon energy of EOD1. The cross-section ratio and the average energy gain, or loss, are obtained with a linear-linear interpolation in Table I. The numerical values in Table I compare favorably to those reported by Fraley.[6]

The total Compton cross section in barns per electron in the laboratory system may be obtained by multiplying the cross section ratio by the zero temperature Klein-Nishina expression. This may be done in the code by following the CALL COMET (1) statement with TCS = 0.4991*CKLN(T1)*CMTCS, where T1 is the photon energy in the laboratory system, CMTCS is the cross-section ratio previously returned by COMET, and CKLN is a function routine.

The average photon energy exchange as obtained by Monte Carlo sampling with COMET has been compared to the corresponding numerical values in Table I for a number of incident photon energies and electron temperatures. These comparisons agreed within statistical errors. A calculation was also made of the average cosine of the scattering angle as a function of the emerging photon energy for an incident photon energy of 20 keV. There was no significant difference between the Monte Carlo results and numerical calculations.

VII. CONCLUSIONS

The proposed implicit Monte Carlo scheme exhibits significant stability advantages over a pure explicit calculation. This stability advantage has also been reported in previous calculations by Fleck and Cummings[1] using a different implicit method than the method proposed here.

In deriving the implicit scheme reported here, we have sampled directly from density functions without making simplifying assumptions whenever possible. This resulted in a more involved sampling scheme than that obtained through approximating exponentials by first-order expansions and by time centering. The small increase in computational effort appears to be more than offset by the advantage of a more rigorous treatment of the time variable.

The simple, pure absorption example problems have indicated the feasibility of using the implicit scheme proposed in Sec. III. We anticipate extending this implicit approach to more complex problems of such a nature that the real scattering treatment given in Sec. V would be used with the treatment of inverse Compton scattering as discussed in Sec. VI.

A basic statistical problem in computing nonlinear radiative transport with an implicit approach is in the scoring of energy deposition. Each estimator tends to suffer from some disadvantage. For example, the path-length estimator, as used in the example problems, does not conserve energy. However, energy is conserved with a collision estimator, but statistical errors are large in thin cells. These considerations indicate that the use of a modified collision estimator should be examined. One possibility is to sample the distance to a collision point with the cross section $(1 - f)\,\mu_a(\nu)$ and to multiply the photon weight by the factor

$$e^{-\int_0^s f\mu_a(\nu)ds}$$

after each flight path. The change in the photon energy is then deposited in the respective cells. Since the factor $(1 - f)$ changes along a flight path, the sampling from the cross section $(1 - f)\mu_a(\nu)$ requires some special considerations. The technique proposed in Ref. 7 for sampling distances to collision points with varying total cross sections is applicable. This method of depositing energy is presently being investigated.

TABLE I

COMPTON CROSS SECTION SCALING FACTOR AND AVERAGE PHOTON ENERGY LOSS

Photon[a] Energy	Electron Temperature[a] 0.00	.0400	.0800	.1200	.1600	.2000	.2400	.2600	.3200	.3600	.4000
0.00	1.0000	1.0000	1.0000	1.0000	1.0000	1.0000	1.0000	1.0000	1.0000	1.0000	1.0000
	0.0000	- .1765	- .3875	- .6355	- .9223	-1.2495	-1.6185	-2.0304	-2.4860	-2.9870	-3.5330
.04	1.0000	.9931	.9861	.9789	.9718	.9646	.9575	.9504	.9434	.9364	.9295
	.0368	- .1132	- .2867	- .4836	- .7037	- .9466	-1.2117	-1.4984	-1.8060	-2.1340	-2.4810
.08	1.0000	.9882	.9764	.9648	.9533	.9419	.9309	.9200	.9094	.8991	.8891
	.0681	- .0624	- .2100	- .3741	- .5542	- .7495	- .9594	-1.1832	-1.4200	-1.6700	-1.9320
.12	1.0000	.9847	.9696	.9548	.9404	.9264	.9129	.8998	.8871	.8748	.8630
	.0953	- .0202	- .1490	- .2903	- .4435	- .6081	- .7833	- .9686	-1.1635	-1.3674	-1.5799
.16	1.0000	.9820	.9645	.9475	.9311	.9153	.9001	.8854	.8714	.8578	.8448
	.1191	.0154	- .0990	- .2234	- .3572	- .5000	- .6512	- .8102	- .9767	-1.1503	-1.3304
.20	1.0000	.9800	.9606	.9420	.9241	.9070	.8905	.8748	.8598	.8453	.8315
	.1402	.0460	- .0570	- .1683	- .2874	- .4139	- .5473	- .6871	- .8330	- .9846	-1.1416
.24	1.0000	.9784	.9576	.9377	.9187	.9005	.8832	.8667	.8508	.8357	.8213
	.1591	.0728	- .0210	- .1219	- .2294	- .3432	- .4628	- .5877	- .7179	- .8528	- .9922
.28	1.0000	.9771	.9552	.9343	.9144	.8954	.8774	.8602	.8438	.8281	.8132
	.1761	.0966	.0104	- .0820	- .1801	- .2836	- .3921	- .5053	- .6229	- .7446	- .8702
.32	1.0000	.9761	.9532	.9315	.9109	.8913	.8726	.8549	.8380	.8219	.8065
	.1917	.1178	.0381	- .0471	- .1374	- .2324	- .3319	- .4354	- .5428	- .6538	- .7681
.40	1.0000	.9744	.9502	.9272	.9054	.8848	.8652	.8466	.8289	.8122	.7962
	.2191	.1544	.0850	.0111	- .0669	- .1486	- .2339	- .3225	- .4142	- .5086	- .6058
.50	1.0000	.9730	.9474	.9233	.9004	.8788	.8583	.8390	.8206	.8031	.7865
	.2480	.1921	.1322	.0689	.0022	- .0675	- .1401	- .2152	- .2927	- .3725	- .4543
.75	1.0000	.9706	.9428	.9166	.8920	.8687	.8467	.8259	.8062	.7876	.7699
	.3036	.2618	.2174	.1707	.1217	.0708	.0181	- .0364	- .0923	- .1498	- .2085
1.00	1.0000	.9689	.9396	.9120	.8860	.8615	.8385	.8167	.7961	.7767	.7582
	.3445	.3113	.2762	.2393	.2008	.1608	.1195	.0769	.0332	- .0115	- .0572
1.50	1.0000	.9663	.9347	.9051	.8772	.8511	.8265	.8033	.7815	.7610	.7415
	.4026	.3794	.3549	.3293	.3026	.2749	.2463	.2169	.1868	.1560	.1245
2.00	1.0000	.9644	.9311	.9000	.8708	.8435	.8178	.7937	.7711	.7498	.7297
	.4431	.4255	.4070	.3876	.3674	.3464	.3248	.3025	.2797	.2564	.2326
2.50	1.0000	.9630	.9284	.8960	.8659	.8376	.8112	.7864	.7631	.7413	.7207
	.4735	.4596	.4448	.4294	.4133	.3965	.3793	.3615	.3433	.3247	.3057
3.00	1.0000	.9618	.9261	.8929	.8619	.8330	.8059	.7806	.7569	.7346	.7135
	.4975	.4861	.4740	.4612	.4479	.4341	.4199	.4052	.3901	.3747	.3589
4.00	1.0000	.9600	.9227	.8882	.8560	.8260	.7981	.7720	.7475	.7246	.7031
	.5335	.5253	.5165	.5073	.4976	.4876	.4771	.4664	.4553	.4440	.4324

[a]Electron Rest Mass Units.

APPENDIX A

A MORE GENERAL IMPLICIT METHOD IN THE ABSENCE OF SCATTERING

A. General Considerations

The technique discussed in this section parallels the method of Sec. III except that the initial condition $u_r(\underline{r},t^o)$ is used for a number of subsequent time intervals. The initial time will again be designated as t^o and the subsequent boundaries of the time intervals will be designated as t^1, t^2, ..., t^n, ..., t^{N+1}. Then for each time interval, σ_p and β are extrapolated as

$$\sigma_p(\underline{r},t) = \sigma_p(\underline{r},t^n)\, e^{-C_1^n(t-t^n)/(t^n-t^{n-1})}, \quad t^n \le t \le t^{n+1}, \quad n = 0, 1, \ldots, N, \tag{A-1}$$

$$\beta(\underline{r},t) = \beta(\underline{r},t^n)\, e^{C_1^n(t-t^n)/(t^n-t^{n-1})}, \quad t^n \le t \le t^{n+1}, \quad n = 0, 1, \ldots, N, \tag{A-2}$$

$$C_1^n = \frac{1}{2}\,\ell n\left[\frac{\sigma_p(\underline{r},t^{n-1})\,\beta(\underline{r},t^n)}{\sigma_p(\underline{r},t^n)\,\beta(\underline{r},t^{n-1})}\right], \quad n = 0, 1, \ldots, N, \tag{A-3}$$

where these are generally cell-averaged quantities and where the superscript is used to denote the time interval.

These definitions serve to specify the source terms in Eq. (14) so that the sampling scheme may be constructed as given in Sec. III, the only difference being that the initial condition has been altered slightly. Rather than repeat such a derivation, we give the results for all but the first time interval. The first time interval (denoted by $n = 0$) is treated exactly as described in Sec. III because the initial condition for this time interval has not changed. The term containing S is not considered here since its time-dependent form varies from problem to problem.

The total photon energy per unit volume produced by the $u_r(\underline{r},t^o)$ source term is given by

$$D_1^n = \frac{c\,\sigma_p(\underline{r},t^n)\,u_r(\underline{r},t^o)\,e^{-\left[\sum_{i=0}^{n-1} c\beta(\underline{r},t^i)\sigma_p(\underline{r},t^i)(t^{i+1}-t^i)\right]}}{C_2^n}\left[1 - e^{-C_2^n(t^{n+1}-t^n)}\right], \quad n = 1, 2, \ldots, N, \tag{A-4}$$

where C_2^n is defined as

$$C_2^n = c\,\sigma_p(\underline{r},t^n)\,\beta(\underline{r},t^n) + \frac{C_1^n}{(t^{n+1}-t^n)}. \tag{A-5}$$

For a given time interval n and cell j, the energy $D_{1j}^n \Delta V_j$ is distributed to a number of source photons. The initial time for each of these photons is sampled as

$$t = t^n - \frac{1}{C_2^n}\,\ell n\left\{1 - \xi\left[1 - e^{-C_2^n(t^{n+1}-t^n)}\right]\right\}, \tag{A-6}$$

the initial position is selected randomly within the cell, the initial direction of flight is selected from the density function $\mu_a(\nu)\, b_\nu/\sigma_p$ as evaluated at the beginning of the time interval.

The implicit source term will now be considered. A photon collision is assumed to occur at a time interval m so that $t^m \le t' \le t^{m+1}$. Due to this collision, the photon energy produced in this time interval is

$$D_2^m = \frac{c\,\sigma_p(\underline{r},t^m)\,\beta(\underline{r},t^m)}{C_2^m} W_i\left[1 - e^{-C_2^m(t^{m+1}-t^m)}\right]. \tag{A-7}$$

The collision may be treated as a pseudoscattering event as discussed on p. 5 for a base time t^m rather than t^o. The new photon time after the collision is sampled as

$$t = t' - \frac{1}{C_2^m} \ell n \left\{ 1 - \xi \left[1 - e^{-C_2^m (t^{m+1} - t^m)} \right] \right\} \quad . \quad \text{(A-8)}$$

However, the initial condition on $u_r(\underline{r}, t^o)$ is not respecified at t^{m+1} unless m = N, therefore this collision may also produce photons during subsequent time steps. To allow for this, an implicit photon bank is established. At such a collision, with probability

$$e^{-c\beta(\underline{r}, t^m)\ \sigma_p(\underline{r}, t^m)(t^{m+1} - t')} \quad , \quad \text{(A-9)}$$

a photon is stored in the implicit bank with a corresponding weight

$$D_2^{m+1} = cW\beta(\underline{r}, t^m)\ e^{C_1^m \left(\frac{t' - t^m}{t^{m+1} - t^{m-1}} \right)} \quad \text{(A-10)}$$

and its spatial coordinates are also put into the bank. Then during the next time step, such a photon produces the photon source energy

$$\frac{D_2^{m+1}\ \sigma_p(\underline{r}, t^{m+1})}{C_2^{m+1}} \left[1 - e^{-C_2^{m+1}(t^{m+2} - t^{m+1})} \right] \quad \text{(A-11)}$$

with the initial photon time selected as

$$t = t^{m+1} - \frac{1}{C_2^{m+1}} \ell n \left\{ 1 - \xi \times \left[1 - e^{-C_2^{m+1}(t^{m+2} - t^{m+1})} \right] \right\} \quad . \quad \text{(A-12)}$$

The total photon energy of Eq. (A-11) may be distributed uniformly to an integer number of photons to conserve expected weights. These then become a real photon source for the time step. In addition, with probability

$$e^{-c\beta(\underline{r}, t^{m+1})\ \sigma_p(\underline{r}, t^{m+1})(t^{m+2} - t^{m+1})} \quad , \quad \text{(A-13)}$$

a photon is retained in the implicit bank with weight $D_2^{m+2} = D_2^{m+1}$. If the photon is retained in the bank [i.e., survives the probability check of Eq. (A-13)], at the next time step m is advanced by one and the steps represented by Eqs. (A-11) to (A-13) are repeated. In all cases, the direction of flight of the implicit source is selected isotropically and the frequency is selected from the density function $\mu_a(\nu) b_\nu / \sigma_p$ as evaluated at the beginning of the current time interval of interest.

B. Summary of the More General Implicit Method

This general implicit method is clearly more complicated than the method described in Sec. III although the computation time required per photon history may not differ greatly for the two methods. The programming effort required appears to be considerably different. The major difference is the requirement for an implicit photon bank, which adds one more complication to a computer program already complicated with a constant maze of data manipulations.

The scheme discussed in this appendix does have definite advantages, but in view of the disadvantages (especially programming), it seems prudent to gain more experience with the method of Sec. III before trying this more general approach.

APPENDIX B

SAMPLING FROM THE KLEIN-NISHINA DIFFERENTIAL CROSS SECTION

A scheme to sample an emerging photon energy from the Klein-Nishina differential cross section is given in Fig. B-1. β is the incident photon energy in units of the rest mass of the electron, β' is the emerging energy selected, and μ is the cosine of the scattering angle. Three different methods are used depending upon the incident energy of the photon: $0 < \beta < 0.4$, $0.4 < \beta < 2.9$, $2.9 < \beta$. For $0.4 < \beta < 2.9$, a rejection method proposed by Kahn in an unpublished report and summarized by Goertzel and Kalos[8] (with errors) is used. For $\beta < 0.4$, a rejection technique that is more efficient for small β is used. For $\beta > 2.9$, the Klein-Nishina cross section is expressed as a linear sum of four density functions. All coefficients in the linear sum are positive so that in a Monte Carlo sampling one of the four density functions is selected randomly with a probability proportional to its coefficient. The final energy is then selected from that density function. This sampling may be done analytically for all four density functions.

APPENDIX C

TRANSFORMATION FROM ELECTRON REST FRAME TO LABORATORY SYSTEM

The selection of the electron velocity was discussed in Sec. VI. Here, we will summarize some useful transformation properties between the laboratory frame, denoted as the $\sum'$ frame, and the rest frame of the electron, denoted as the $\sum_e$ frame. The basic mathematical relationships are lifted directly from Everett's Relativity Notebook.[5] His notation will also be used here.

The interaction in the $\sum'$ frame is depicted in Fig. C-1. Here, the electron velocity has arbitrarily been chosen to be in the negative x-axis direction. Then from Eq. (V), Ref. 5, p. 24, the electron velocities in $\sum_e$ are

$$v_{x1} = \left(v'_{x1} + u_o\right) \Big/ \left(1 + \frac{u_o^2}{c^2}\right) = 0 \qquad \text{(C-1)}$$

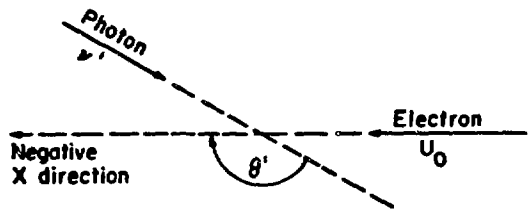

Fig. C-1. Photon scattering off of electron in $\sum'$ frame.

$$v_{y1} = 0 \qquad \text{(C-2)}$$

$$v_{z1} = 0 \quad , \qquad \text{(C-3)}$$

where the subscript 1 denotes the electron. The momenta of the photon in the $\sum'$ frame are

$$p'_{x2} = -\frac{h\nu'}{c} \cos\theta' \quad , \qquad \text{(C-4)}$$

$$p'_{y2} = -\frac{h\nu'}{c} \sin\theta \quad , \qquad \text{(C-5)}$$

and

$$p'_{z2} = 0 \quad , \qquad \text{(C-6)}$$

where the subscript 2 denotes the photon and it is arbitrarily put in the x-y plane. The momenta of the photon in the $\sum_e$ frame may be obtained from Eq. (PM), Ref. 5, p. 30, as

$$p_{x2} = \lambda\left(p'_{x2} + \frac{u_o p'}{c}\right) = \frac{\lambda h\nu'}{c}\left(-\cos\theta' + \frac{u_o}{c}\right) , \qquad \text{(C-7)}$$

$$p_{y2} = p'_{y2} = \frac{-h\nu'}{c} \sin\theta' \quad , \qquad \text{(C-8)}$$

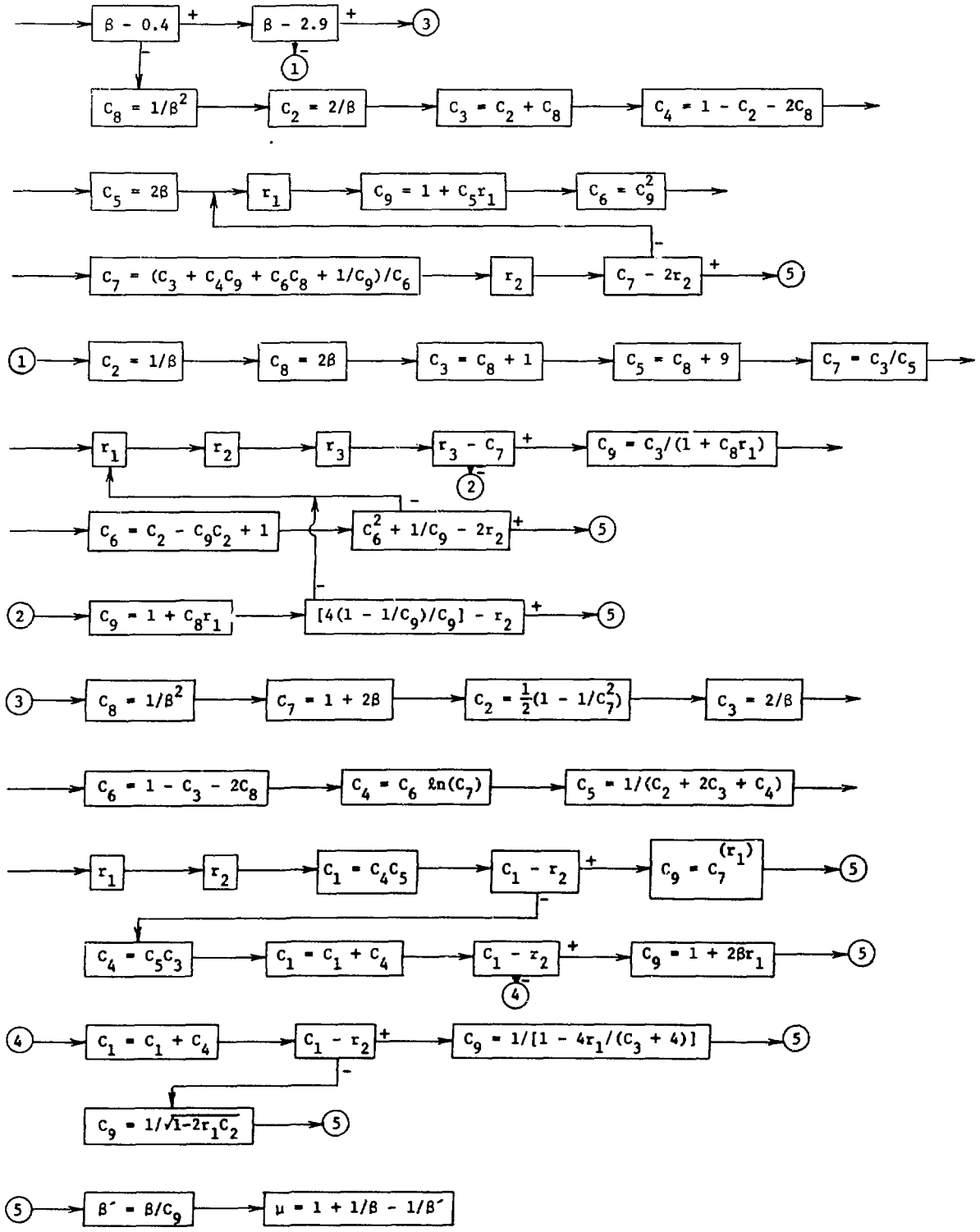

Fig. B-1. Scheme for sampling the Klein-Nishina differential cross section.

and

$$p_{z2} = p'_{z2} = 0 \quad . \tag{C-9}$$

The energy of the photon E_2 in the $\sum_e$ frame may be obtained from Eq. (cPE), Ref. 5, p. 31, as

$$E_2 = \lambda\left(\frac{u_o}{c} cp'_{x2} + E'_2\right) = \lambda h\nu'\left(\frac{-u_o}{c}\cos\theta' + 1\right) . \tag{C-10}$$

This equation is used to compute the incident photon energy in the electron rest frame for the subsequent selection of the new energy and scattering angle from the Klein-Nishina differential cross section in this rest frame.

The precollision photon direction of flight in the $\sum_e$ frame may be obtained from Eq. (Ψ), Ref. 5, p. 25, as

$$a_{x2} = \left(a'_{x2} + \frac{u_o}{v'_2}\right)\Big/\left(\frac{v_2}{v'_2}\right)\left(1 + \frac{u_o v'_2 a'_{x2}}{c^2}\right)$$

$$= \left(-\cos\theta' + \frac{u_o}{c}\right)\Big/\left(1 - \frac{u_o}{c}\cos\theta'\right) \quad , \tag{C-11}$$

$$a_{y2} = \frac{a'_{y2}}{\lambda\frac{v_2}{v'_2}\left(1 + \frac{u_o v'_2 a'_{x2}}{c^2}\right)} = \frac{-\sin\theta'}{\lambda\left(1 - \frac{u_o}{c}\cos\theta'\right)} , \tag{C-12}$$

and

$$a_{z2} = 0 \quad , \tag{C-13}$$

where the a's represent direction cosines. Assume that in the selection from the Klein-Nishina, with incident energy E_2, the cosine of the scattering angle was μ_s and the aximuth angle selected was δ. Then the final direction cosines in the $\sum_e$ frame are (Cashwell and Everett,[9] p. 106)

$$a_{x4} = a_{x2}\mu_s - \sqrt{1 - \mu_s^2}\ a_{y2} \sin\delta \quad , \tag{C-14}$$

$$a_{y4} = a_{y2}\mu_s + \sqrt{1 - \mu_s^2}\ a_{x2} \sin\delta \quad , \tag{C-15}$$

and

$$a_{z4} = -\sqrt{1 - \mu_s^2}\cos\delta \quad , \tag{C-16}$$

which may be written as

$$a_{x4} = \frac{1}{\left(1 - \frac{u_o}{c}\cos\theta'\right)}\left[\left(\frac{u_o}{c} - \cos\theta'\right)\mu_s + \frac{\sqrt{1 - \mu_s^2}\sin\theta'\sin\delta}{\lambda}\right] \tag{C-17}$$

and

$$a_{y4} = \frac{1}{\left(1 - \frac{u_o}{c}\cos\theta'\right)}\left[\frac{-\sin\theta'}{\lambda}\mu_s + \sqrt{1 - \mu_s^2} \times \left(\frac{u_o}{c} - \cos\theta'\right)\sin\delta\right] \quad . \tag{C-18}$$

Here, the subscript 4 denotes the emerging photon. The inverse transformation of C-11 to C-13 gives

$$a'_{x4} = \left(a_{x4} - \frac{u_o}{c}\right)\Big/\left(1 - \frac{u_o}{c}a_{x4}\right) \tag{C-19}$$

and

$$a'_{y4} = \frac{a_{y4}}{\lambda\left(1 - \frac{u_o}{c}a_{x4}\right)} \quad . \tag{C-20}$$

The cosine of the angle through which the photon scatters in the $\sum'$ frame is given by μ' as

$$\mu' = a'_{x2}a'_{x4} + a'_{y2}a'_{y4} + a'_{z2}a'_{z4}$$

$$= -\cos\theta' a'_{x4} - \sin\theta' a'_{y4} \quad . \tag{C-21}$$

Combining Eqs. (C-17) through (C-20) into Eq. (C-21) gives

$$\mu' = \left\{-\cos\theta' \left[\left(\frac{u_o}{c} - \cos\theta'\right)\mu_s + \frac{\sqrt{1-\mu_s^2}}{\lambda}\sin\theta'\sin\delta - \frac{u_o}{c} + \frac{u_o^2}{c^2}\cos\theta'\right] - \frac{\sin\theta'}{\lambda} \times \left[-\frac{\sin\theta'}{\lambda}\mu_s + \sqrt{1-\mu_s^2}\left(\frac{u_o}{c} - \cos\theta'\right)\sin\delta\right]\right\} \div \left[1 - \frac{u_o}{c}\cos\theta' - \frac{u_o}{c}\left(\frac{u_o}{c} - \cos\theta'\right)\mu_s - \sqrt{1-\mu_s^2}\,\frac{u_o}{c\lambda} \times \sin\theta'\sin\delta\right]. \quad \text{(C-22)}$$

It is clear that the azimuthal orientation of the electron is random, and hence the azimuthal scattering angle must be random. Therefore, Eq. (C-23) for the laboratory cosine of the scattering angle of the photon along with the selection of a random azimuthal laboratory scattering angle determines the emerging photon direction of the flight in the laboratory system. The final energy in the laboratory system is obtained from the inverse transformation

$$E_4' = \lambda\left(\frac{u_o}{c}cp_{x4} + E_4\right) = \lambda\left(-\frac{u_o}{c}E_4 a_{x4} + E_4\right) = \lambda E_4\left(-\frac{u_o}{c}a_{x4} + 1\right), \quad \text{(C-24)}$$

or from the previous definition of a_{x4},

$$E_4' = \frac{\lambda E_4\left[\left(1 - \frac{u_o}{c}\cos\theta'\right) - \mu_s\frac{u_o}{c}\left(\frac{u_o}{c} - \cos\theta'\right) - \frac{\sin\theta'\sin\delta\sqrt{1-\mu_s^2}\;u_o}{c\lambda}\right]}{\left(1 - \frac{u_o}{c}\cos\theta'\right)} \quad \text{(C-25)}$$

This may be simplified somewhat to

$$\mu' = \left[\mu_s\left(1 - \frac{u_o}{c}\cos\theta' - \frac{u_o^2}{c^2}\sin^2\theta'\right) + \frac{u_o}{c}\cos\theta' \times \left(1 - \frac{u_o}{c}\cos\theta'\right) - \frac{\sin\theta'\sin\delta\sqrt{1-\mu_s^2}\;u_o}{c\lambda}\right] \div \left[\left(1 - \frac{u_o}{c}\cos\theta'\right) - \frac{u_o}{c}\mu_s\left(\frac{u_o}{c} - \cos\theta'\right) - \frac{\sin\theta'\sin\delta\sqrt{1-\mu_s^2}\;u_o}{c\lambda}\right]. \quad \text{(C-23)}$$

It is important to note that in spite of the complexity of the transformations, only Eqs. (C-10), (C-23), and (C-25) are needed in the Monte Carlo. Many of the terms are similar so that relatively few operations are required. Because of this, the majority of the computation time is involved in the selection of the electron velocity and direction.

APPENDIX D

SAMPLING THE ELECTRON VELOCITY

Tables for sampling the electron velocity are stored at the five electron temperatures of kT/m_oc^2 = 0.001, 0.04, 0.1, 0.2, and 0.4. The tables represent equiprobability bins for the kinetic energy so that the i^{th} entry denoted by E_i in a table is computed from the inverse function

$$\frac{i-1}{128} = \frac{e^{-\frac{m_oc^2}{kT}}(kT)^2}{K_2\left(\frac{m_oc^2}{kT}\right)(m_oc^2)^2}\int_0^{E_i}\left(E+\frac{m_oc^2}{kT}\right)\times\sqrt{E^2+\frac{2Em_oc^2}{kT}}\,e^{-E}\,dE \quad , \qquad (D\text{-}1)$$

where a simple transformation has been made from the velocity space of Sec. VI to energy space, i.e., $E = (m_oc^2/kT)(\lambda-1)$. A double linear interpolation is used between point values in the table and between the electron temperatures of the two tables that span the electron temperature of interest. The linear interpolation between tables has satisfactory accuracy. However, at very small kinetic energies or very large kinetic energies, significant errors result from using only 128 equally probable bins. For low energies, the density function varies like $\sqrt{E}$. This is only significant for the first mesh interval $E_1 < E < E_2$ so that in this mesh interval the energy E is selected as

$$E = E_2R^{2/3} \quad , \qquad (D\text{-}2)$$

where R is a random number. The problem is not so easy to correct for large electron kinetic energies. Therefore, the equal probability bins actually differ somewhat from Eq. (D-1) and are given in Table D-I. The use of this bin structure results in an accuracy that is almost as good as that obtained by using an equally probable table of length 1024.

TABLE D-I

BINS FOR SAMPLING ELECTRON ENERGY

Entry Numbers	Probability Increments
1 to 121	1/128
121 to 129	1/256
129 to 137	1/512
137 to 153	1/1024

REFERENCES

1. J. A. Fleck, Jr., and J. D. Cummings, "An Implicit Monte Carlo Scheme for Calculating Time and Frequency Dependent Nonlinear Radiation Transport," J. Computat. Phys. 8, 313-342 (Dec. 1971).
2. J. A. Fleck, Jr., "The Use of Implicit Monte Carlo Radiation Transport with Hydrodynamics and Compton Scattering," Lawrence Radiation Laboratory internal report UCIR-535, 1971.
3. J. A. Fleck, Jr., "The Calculation of Nonlinear Radiation Transport by a Monte Carlo Method," Methods in Computational Physics (Academic Press, New York, 1963), Vol. I.
4. G. C. Pomraning, "High-Temperature Radiative Transfer and Hydrodynamics," Progr. High Temp. Phys. Chem. 4:1-83 (1971).
5. C. J. Everett, "A Relativity Notebook for Monte Carlo Practice," Los Alamos Scientific Laboratory report LA-3839 (1968).
6. G. S. Fraley, "The Integrated Compton Cross Section and Its Use in a Monte Carlo Scheme," Los Alamos Scientific Laboratory report LA-4592 (1971).
7. L. L. Carter, E. D. Cashwell, and W. M. Taylor, "Monte Carlo Sampling with Continuously Varying Cross Sections Along Flight Paths," Nucl. Sci. Eng. 48, 403-411 (1972).
8. G. Goertzel and M. H. Kalos, "Monte Carlo Methods in Transport Problems," Progress in Nuclear Energy (Pergamon Press, New York, 1958), Series 1, Vol. 2.
9. E. D. Cashwell and C. J. Everett, A Practical Manual on the Monte Carlo Method for Random Walk Problems (Pergamon Press, Inc., New York, 1959).

ALT:339(100)